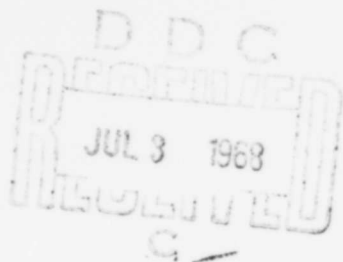4800:12-mc

AD671265

A STATISTICAL INVESTIGATION OF MICROCRACK FORMATION

by

L. E. Kaechele
and
A. S. Tetelman

Department of Materials Science

Stanford University

Stanford, California

April, 1968

D D C
JUL 3 1968
C

SU-DMS Report No. 68-T73

Department of MATERIALS SCIENCE

STANFORD UNIVERSITY

+1

A STATISTICAL INVESTIGATION OF MICROCRACK FORMATION

L. A. Kaechele*† and A. S. Tetelman††

* Consulting Engineer, Topanga, California

† Materials Division, School of Engineering,
  U. C. L. A., Los Angeles, California

† Formally at Department of Materials Science,
  Stanford University, Stanford, California

ABSTRACT

Low temperature tension tests were made with low carbon poly-crystalline iron, in which stable cleavage microcracks form. Probability distributions of the orientation of these cracks were used to investigate the effects of stress and strain on their formation. Since only the surface traces of cracks could be observed experimentally, relationships were developed to give the distribution of the true orientation of these cracks as measured by the direction of the normal to the crack plane.

Simple models for the effect of stress on crack formation were investigated, including the Cottrell-Petch formulation for microcrack formation. Predictions of the probability distribution of crack orientation angles, and from these the distribution of the surface trace angles that should be observed experimentally, were determined for these models.

The experimental results showed a stronger tendency for cracks to form in grains with cleavage plane normals near the tensile axis direction than predicted by the simple models. Statistical analysis of the experimental data led to the conclusion that the crack formation process was strongly dependent on the stress acting across the cleavage plane, this dependence being in the order of the ninth power of the stress. Both the angular distribution of cracks and the total number of cracks as a function of stress were in agreement with this relationship. Grain boundary carbides, which crack and initiate cleavage microcracks in ferrite, may cause this unexpectedly strong stress dependence.

I. INTRODUCTION

Microcrack formation in crystalline solids results from the coalescence or piling up of dislocations. The numerous theoretical treatments of this problem[1,2,3] all indicate that the nucleation stage, at which point the microcrack length is about one-tenth the grain diameter, is shear-stress dependent, but that the initial growth of the crack, out to surrounding grain boundaries, is dependent upon the tensile component of stress acting across the cleavage plane. For example, the Cottrell-Petch[2] theory predicts that initial microcrack growth will occur when

$$\sigma_N \ nb = A \ \gamma_m \tag{1}$$

where n, the number of dislocations in the pile-up, is proportional to the square root of the grain diameter, γ_m is the work done in microcrack formation, $\sigma_N = \sigma \cos^2 \emptyset$ is the normal component of stress acting across a cleavage plane whose pole is oriented at an angle $\emptyset$ to the tensile axis, and A is a constant about equal to 2.

In an idealized, homogeneous, single-phase, polycrystalline solid containing a random distribution of grains having the same size and shape such that γ_m and n are constant, this model predicts that those grains characterized by a low value of $\emptyset$ would have the highest probability of containing grain size microcracks at a given stress level σ, in a simple tensile test. In real materials, local variations in grain size, grain shape, and the orientation of grain boundary precipitates, such as carbides in ferrite, will affect the conditions for the formation of grain size microcracks, and hence will affect the orientation dependence of

microcrack formation at a given applied stress level. For example, in ferrite, microcracks are initiated at cracked grain boundary carbides[4,5]. If the cracking of carbides is, in turn, a stress dependent process, then γ_m will also be a function of stress and the orientation of microcracks will not obey a simple $\sigma \cos^2 \emptyset$ relationship.

Hahn and McMahon and their coworkers[4,5] have conducted some studies of the orientation and stress dependence of microcrack formation in ferrite. Their results indicated that the observed <u>surface traces</u> of microcracks tended to be perpendicular to the tensile axis, apparently confirming the importance of tensile stress in microcrack formation. However, it should be noted that a given surface trace whose normal makes an angle α with the tensile axis does not indicate the true value of $\emptyset$, since the pole of a given cleavage plane may be at any angle between 0 and π with the plane of the surface (Figure 1). Consequently, their trace orientation distributions do not directly indicate the importance of tensile stress in microcrack formation. Furthermore, their tests were not obtained over a sufficient range of conditions to directly determine the stress dependence of microcrack formation in this material.

The present investigation was undertaken to determine the orientation dependence of microcrack formation in ferrite, as a function of stress, strain, and temperature. This material was chosen because non-propagating microcracks, one or two grain diameters in length, can be produced before final fracture[4,5]. In addition, a theoretical statistical model was developed which allowed the determination of the true distribution of crack orientations $p(\emptyset)$ in terms of the observed surface distribution $p(\alpha)$. Both the $p(\emptyset)$ distributions at a given stress level,

- 2 -

and the stress dependence of microcrack formation at all angles $\emptyset$ indicate that the microcrack density varies with the 9th power of the tensile stress, which is much greater than any simple modification of the current dislocation models would predict.

II. EXPERIMENTAL PROCEDURE

The polycrystalline iron used in the experimental program was supplied in the form of cold rolled sheet with an initial thickness of 0.050 inches. The composition of the material is given in Table 1.

Table 1

Composition of Polycrystalline Iron Used in Tensile Tests

Element	Weight Percent
C	0.02
Mn	0.26
Si	0.28
N	0.0026

Specimen blanks were surface ground to a thickness of 0.041 inches and tensile specimens with a gauge section about one inch by 0.20 inches were milled out. Most of the specimens were heat treated at 1150°C for one hour and furnace cooled, producing a grain size of 80 microns. A few specimens were heat treated at 1225°C to produce a coarser grain size, 120 microns. Specimens were then mechanically polished and the gauge section was electropolished. Ferrite grains were quite uniform and equiaxed. Small colonies of pearlite were scattered through the material and smooth films of iron carbide were present at grain boundaries.

Specimens were tested in a cold chamber[6] in which liquid nitrogen was sprayed from a perforated tube surrounding the specimen and grips. Temperature was recorded from a copper-constantan thermocouple clipped to the specimen and controlled by a solenoid valve in the liquid nitrogen supply line. Tensile tests were made on an Instron testing machine, with the load on the specimen and the deflection of the cross-head of the testing machine recorded automatically on a strip chart. Stress data were determined from the load record on the strip chart and measured or computed cross-sectional areas of the test specimens. Plastic strains were determined from the deflection recorded on the strip chart and the length of the plastically deformed section on the specimen.

After testing, 3 to 4 mils were ground from the specimens, to remove grains that had been exposed on the free surface and thus avoid surface effects. Specimens were then mechanically polished and electropolished. The appearance of microcracks after this surface preparation is shown in Figure 2.

Microcrack counts were made by scanning the prepared surface in slightly overlapping passes in the direction of the tensile axis at a magnification of 200X. Crack trace angles were measured to the nearest degree by rotating the microscope stage to align the trace with a cross hair, then reading the angle on the scale on the stage.

III. EXPERIMENTAL RESULTS

A survey investigation over a range of temperature was made to describe the mechanical properties of the material and to aid in selecting temperatures for further investigation of microcrack formation. The

data from this initial test series are shown in Figure 3. The microcrack counts were made on the as-tested surface.

On the basis of Figure 3, three temperatures were selected for the microcrack study, $-165^{\circ}C$, $-180^{\circ}C$ and $-196^{\circ}C$. These temperatures covered the range in which the maximum number of microcracks appeared, included both brittle fracture behavior and fairly ductile failure with appreciable necking, and permitted tests to be run at the same levels of stress and strain at different temperatures. It can be seen from the figure that the range between lower yield stress and maximum uniform true stress overlaps for the three temperatures.

The survey tests were made with a cross-head speed of 0.5 inches per minute while the speed for the microcrack test specimens was 0.2 inches per minute, to facilitate stopping the tests at selected amounts of strain. Relevant data from the microcrack specimens were plotted in Fig. 3, showing little effect from this change in strain rate.

At $-196^{\circ}C$ all tests were run to fracture, which occurred with no indication of necking. At the higher temperatures, one or two specimens were tested to failure. Subsequent tests were stopped at varying amounts of strain -- just after upper yield, at completion of the Lüder strain, and at intervals between that point and the point of maximum uniform extension.

The raw data for each specimen consisted of the number of cracks observed on the uniformly strained part of the flat surfaces of the specimen, after removing a layer about equal to the average grain diameter (80 microns). The orientation of each crack was measured and they were grouped in five-degree increments of the angle α between the crack trace

- 5 -

and a line on the surface perpendicular to the tensile axis. The raw data are presented in Figure 4 for the 80-micron grain size material. In addition, tests were made at -180°C and -165°C in which the specimen was unloaded immediately after the upper yield point. No microcracks were found in these two specimens, confirming previous observations[4,5] that microcracks do not appear in this type of material until there has been some plastic strain.

In order to investigate the probability distributions of trace angles, the data were converted to the fraction of the total cracks found in each 5° interval on the specimen. The trace orientation distributions in the form of cumulative distributions (the fraction of cracks with surface trace angles equal to or less than a specified angle) are shown in Figure 5. The cumulative curve integrates the distribution curve and smooths the data. The two curves for each temperature are the boundaries of the cumulative plots of the distributions for all specimens at that temperature. The cumulative data are quite uniform, independent of the stress or strain levels producing the cracks and of test temperature. A marked tendency for crack traces to appear at low angles is apparent -- over half the surface traces observed had normals inclined at less than 10° with the tensile axis.

The similarity to each other of the experimental trace angle distributions, independent of stress, strain and temperature, suggests the possibility that all the data might be combined and treated as a statistical whole. A χ^2 test of homogeneity showed that the data can be considered to have been drawn from the same parent distribution. The probability of the computed χ^2 value being exceeded was found to be over 80%.

- 6 -

Since the trace angle distribution was found to be statistically independent of stress in these tests, the true crack plane orientation distribution, $p(\emptyset)$, must also be independent of stress.

If the number of cracks formed (per unit angle) is a function of axial stress σ and the angle $\emptyset$ at which they form, it follows from the preceding that this function, $N(\sigma,\emptyset)$, must be the product of separate functions of axial stress $G(\sigma)$ and angle $\emptyset$, $H(\emptyset)$. (The number formed will depend on the number of available cleavage planes at various angles, so $H(\emptyset)$ must include a function describing the angular distribution of cleavage planes.) A simple, physically meaningful quantity related to axial stress and angle is the normal stress across a cleavage plane, σ_N, which is the product of the axial stress σ and the square of the cosine of the angle $\emptyset$ between the crack plane normal and the tensile axis. If it is assumed that the number of cracks that form at any angle depends on the normal stress across the plane, it is well known that the only function of the normal stress that leads to the required product of functions of axial stress and angle is a power function of the normal stress. Consequently, with that assumption the distribution of crack plane orientations obtained in these tests depends on some power m of the normal stress across the crack plane and hence

$$N(\sigma,\emptyset) = A(\sigma \cos^2\varphi)^m \, g(\emptyset) \qquad (2)$$

where $g(\emptyset)$ is the function describing the angular distribution of available cleavage planes. The probability distribution of crack plane normals, $p(\emptyset)$, depends only on the variable $\emptyset$, and is therefore proportional to the product of the 2m power of cos $\emptyset$ and the function $g(\emptyset)$.

- 7 -

From relationships presented in the appendix, it is possible to determine the form of the surface trace angle distribution $p(\alpha)$ that results from a true crack plane angle distribution $p(\emptyset)$ that is determined by a power m of the normal stress acting across the cleavage planes. For random grain orientation, the trace angle distribution is found to be a cosine power law with the power twice that of the power m of the normal stress across cleavage planes that determined the distribution $p(\emptyset)$[6]. (The cleavage plane availability function $g(\emptyset)$ is taken as sin $\emptyset$, see Section IV. Departure from this form above $\pi/4$ has negligible effect on $p(\emptyset)$ for large values of m.)

The power of the cosine that best fits the experimental surface trace distribution $p(\alpha)$ was found by using Cramer's maximum likelihood estimation[7]. Values of the power were computed for several groupings of the data; the combined data from all tests, the data for each of the three test temperatures, and the data from all tests divided into two groups -- a high stress group and a low stress group. For the combined data the value of the power 2m was 17.8 and it ranged from 17.1 to 18.9 for the other groups. From these results, the formation of microcracks in these tests depends on the normal stress across the crack plane raised to a power in the vicinity of 9.

A modified χ^2 "goodness of fit" test was also made, using trace angle intervals only up to 25 or 30° (which excludes less than 7 and 3% of the total crack count, respectively). The results confirmed the maximum likelihood computations, supporting the conclusion that microcrack production in these tests appears to be governed by about a ninth power of the normal stress acting across cleavage planes.

A comparison between predicted trace angle distributions from the stress power model and the experimentally observed trace distribution is shown in Figure 6, demonstrating agreement with the ninth power of stress. (The limit previous data on trace angle distributions[4,5] are quite similar to the histogram in Figure 6.)

In addition to determining the power of stress dependence of microcrack formation from microcrack orientation distributions, it is possible to determine this power dependence directly from a plot of total crack density $N(\sigma)$, as a function of applied stress. Figure 7 shows the number of cracks observed per square inch as a function of the maximum uniform true stress to which the specimen was subjected. It is noted that the data from the present work at all test temperatures is consolidated and that $N(\sigma)$ is proportional to σ^9, confirming the conclusions reached from the orientation distribution.

To assess the effect of grain size on microcrack formation, a few tests were made at -165 and -196°C with the larger (120 micron) grain size material. The results of these tests are also shown in Figure 7, and it appears that although more cracks are formed at a given stress level in the coarser grained material, the stress dependence of microcrack formation remains unchanged.

To summarize, these results indicate that

$$N(\sigma) = A\sigma^9 \tag{3}$$

where A increases with increasing grain size.

Figure 2 indicates that the number of microcracks observed on fractured specimens increases as the test temperature is lowered below

-150°C, reaches a maximum at -180°C, and then decreases as the temperature is lowered to -196°C. Hahn et al[4] and McMahon and Cohen[5] also noted a similar effect. In view of the strong stress dependence of microcrack formation (Figure 7), we believe that this effect is due to the temperature dependence of the maximum uniform true stress, which follows a similar trend. Between -196°C and approximately -185°C the maximum uniform stress and the fracture stress are coincident, so that the microcrack density observed on fractured specimens is dependent on the stress level at which large scale, unstable microcrack growth can occur. The reasons for the increasing fracture stress with increasing temperature in this temperature range are unknown, but may be related to an increasing density of twins, which act as barriers to crack growth[5] and refine the effective grain size. Above -185°C necking precedes fracture and the temperature dependence of the maximum uniform stress is determined primarily by the temperature dependence of the yield stress, which decreases with increasing temperature.

Hahn et al[4] and McMahon and Cohen[5] also noted that the crack density increased with increasing plastic strain, with the form of the functional relationship apparently changing with temperature. We, too, have noted a similar effect (Figure 8). However, we believe that the lack of consolidation of the data is simply a reflection of the fact that the tensile yield strength, and hence the tensile stress level at a given plastic strain, increases with decreasing test temperature, and that the independent variable that determines the number of microcracks is stress rather than strain.

IV. DISCUSSION

The experimental results presented above indicate that microcrack formation in ferrite is strongly stress dependent. It is of interest, then, to compare these results with some simple models for microcrack formation, such as a critical stress model in which grain cleavage occurs when the normal stress reaches a critical value (e.g., the Cottrell-Petch model described by Equation (1)).

In any model, the distribution of microcrack orientations will depend upon the availability of cleavage planes, as well as on the physical factors that determine the mechanism of the cracking process. In iron, cleavage occurs on one of three mutually perpendicular {100} planes. The distribution of the orientation of any one of these cleavage planes is represented by $\sin \emptyset$ if grain orientation is uniformly likely in all possible directions. However, when $\emptyset$ is larger than $\cos^{-1}(\sqrt{3}/3) = 54°44'$, corresponding to a <111> direction coinciding with the tensile axis, one (or both) of the other cleavage planes will be more nearly normal to the tensile axis, and hence will be more likely to cleave.

The distribution for the <u>cleavage plane most nearly normal to the tensile axis</u>, and hence the one of interest in the cleavage process, is, in a random, polycrystalline aggregate[6],

$$g(\emptyset) = 3 \sin \emptyset \qquad (4)$$

for $\emptyset \le \pi/4$ and

$$g(\emptyset) = 3 \sin \emptyset - \frac{12}{\pi} \sin \emptyset \cos^{-1} (\cot \emptyset) \qquad (5)$$

for $\pi/4 \le \emptyset \le \cos^{-1} (\sqrt{3}/3)$.

The fraction of cleavage planes most nearly normal to the tensile

axis with normals between 0 and $\pi/4$ from it can be found by integrating the probability function over this range,

$$\int_0^{\pi/4} 3 \sin \varphi \, d\varphi = .879 \quad .$$

Thus most of the planes lie in this region, where the probability distribution is a simple sine function. The probability distribution for the entire range is shown in Figure 9.

In real materials, grain orientation is seldom truly uniform. Cold rolling of iron produces preferred orientation which may persist through heat treatment in the austenizing region[8]. An x-ray diffraction analysis of the distribution of cleavage plane orientations in the test material was made. The amount of preferred orientation was found to have only a slight effect on the orientation distribution of crack planes[6] and can be neglected here.

Models for Microcrack Formation

a) Critical Stress Model

The simplest model for microcrack formation is the critical stress model, in which a certain fraction of grains cleave when the normal stress $\sigma_N = \sigma \cos^2 \emptyset$ across cleavage planes in them reaches a critical value, σ^*. When $\sigma = \sigma^*$, cracks form in those grains that have cleavage planes oriented perpendicular ($\emptyset = 0^o$) to the tensile axis. Further increases in stress cause cracks to form in grains in which $\emptyset$ is greater than zero but less than $\emptyset^*$, where $\emptyset^*$ is given by

$$\sigma \cos^2 \varphi^* = \sigma^* \ ,$$

$$\varphi^* = \cos^{-1} \sqrt{\sigma^*/\sigma} \tag{6}$$

At the maximum value of applied stress, σ_{max}, as determined by fracture, tensile instability, or removal of the load, cracks will occur on cleavage planes that are inclined up to an angle $\emptyset^*_{max}$ with the tensile axis. From equation (6),

$$\emptyset^*_{max} = \cos^{-1} \sqrt{\sigma^*/\sigma_{max}} \quad . \tag{7}$$

The probability distribution $p(\emptyset)$ for the orientation of internal cracks that form at a given level of applied stress $\sigma^* < \sigma < \sigma_{max}$ will have the form of the distribution of cleavage planes most nearly normal to the tensile axis, as shown in Figure 9. For $\emptyset \le \pi/4$, this is a simple sine function (eqn. (4)) so that

$$p(\emptyset) = B \sin \emptyset \quad . \tag{8}$$

The value of B is determined by the requirement that the integral of the distribution over the appropriate range of $\emptyset$ from 0 to $\emptyset^*_{max}$ be equal to unity. Defining $R = \sigma_{max}/\sigma^*$ we have

$$\int_0^{\emptyset^*_{max}} p(\varphi) \, d\varphi = \int_0^{\cos^{-1}(1/\sqrt{R})} B \sin \varphi \, d\varphi = B \left(1 - \frac{1}{\sqrt{R}}\right) = 1 \tag{9}$$

so that

$$B = \frac{\sqrt{R}}{\sqrt{R} - 1} \tag{10}$$

and hence

$$p(\varphi) = \frac{\sqrt{R}}{\sqrt{R} - 1} \sin \varphi \quad . \tag{11}$$

The distribution of orientation of observed surface traces predicted by this critical stress model can be obtained from the $p(\emptyset)$ to $p(\alpha)$ transformation described in the appendix. From eqn. (A5) we have

- 13 -

$$p(\alpha) = \frac{2}{\pi} \int_{\alpha}^{\phi^*_{max}} \frac{p(\varphi) \cos \varphi \, d\varphi}{\cos \alpha \sqrt{\cos^2 \alpha - \cos^2 \varphi}} \,. \tag{A5}$$

Introducing eqn. (11) and integrating gives

$$p(\alpha) = \frac{2\sqrt{R} \sqrt{\cos^2 \alpha - \cos^2 \varphi^*_{max}}}{\pi \cos \alpha \, (\sqrt{R} - 1)} \,. \tag{12}$$

The distribution of $\emptyset$ and the corresponding distribution of α are shown in Figure 10 for two values of the ratio R of maximum tensile stress to critical stress for crack formation. It is interesting to note that microcracks are increasingly frequent as the angle $\emptyset$ increases (because more cleavage planes are available at the higher angles, Fig. 9), while surface traces are more likely to appear at low values of the trace angle α.

The experimental measurement of the trace angle distribution is also shown in Fig. 10. It is noted that the predictions of the critical stress model are not in satisfactory agreement with the tendency for experimental data to concentrate at low angles.

b) Linear Stress Model

In this more complicated model, microcracks are assumed to begin forming when the normal stress $\sigma_N = \sigma \cos^2 \emptyset$ across cleavage planes reaches a critical value σ^*, and additional cracks form on planes at the same angle as the stress increases. In the linear model, the crack density increases linearly with the amount of normal stress above the critical level $(\sigma_N - \sigma^*)$. The probability distribution for cracks with normals at an angle $\emptyset$ to the tensile axis is then proportional to the product of the distribution of cleavage planes (a sine function as shown in eqn. (4) for $\emptyset \leq \pi/4$ in a random polycrystal) and $(\sigma_N - \sigma^*)$,

- 14 -

$$p(\varphi) \propto \sin \varphi \ (\sigma_N - \sigma^*)$$

$$= K \sin \varphi \left(\frac{\sigma_N}{\sigma^*} - 1 \right)$$

$$p(\varphi) = K \sin \varphi \left(\frac{\sigma \cos^2 \varphi}{\sigma^*} - 1 \right) \tag{13}$$

where σ^* has been absorbed in the constant K. The value of K is found by evaluating the cumulative probability when the stress σ and critical angle $\emptyset^*$ are at their maximum values, (with R again defined as σ_{max}/σ^* and $\emptyset^*_{max}$ defined by eqn. (7)),

$$P(\varphi^*_{max}) = \int_{o}^{\varphi^*_{max}} p(\varphi) \ d\varphi = 1$$

$$= K \int_{o}^{\varphi^*_{max}} \sin \varphi \left(\frac{\sigma_{max} \cos^2 \varphi}{\sigma^*} - 1 \right) \ d\varphi$$

$$= K \int_{o}^{\cos^{-1}(1/\sqrt{R})} \sin \varphi \ (R \cos^2 \varphi - 1) \ d\varphi$$

$$= K \left(\frac{2 + R \sqrt{R} - 3\sqrt{R}}{3\sqrt{R}} \right) \tag{15}$$

and therefore

$$K = \frac{3\sqrt{R}}{2 + R \sqrt{R} - 3\sqrt{R}} \ . \tag{16}$$

The probability distribution for the orientation of internal cracks according to this model is then

$$p(\varphi) = \frac{3\sqrt{R} \sin \varphi \ (R \cos^2 \varphi - 1)}{2 + R \sqrt{R} - 3\sqrt{R}} \ . \tag{17}$$

From eqn. (A5), the distribution of orientation of surface traces predicted by this model is

$$p(\alpha) = \frac{2}{\pi} \int_{\alpha}^{\varphi^*_{max}} \frac{p(\varphi) \cos \varphi \ d\varphi}{\cos \alpha \ \sqrt{\cos^2 \alpha - \cos^2 \varphi}} \tag{A5}$$

and with the distribution for $p(\emptyset)$ from eqn. (17),

$$p(\alpha) = \frac{4R^{3/2}}{\pi \cos \alpha \ (2 + R \sqrt{R} - 3/R)} \ (\cos^2 \alpha - 1/R)^{3/2} \ . \qquad (18)$$

Some probability distributions for internal crack orientation and surface trace orientation are shown in Figure 11. Again, the model fails to predict the observed bias of the experimental data toward low angle surface traces.

The models discussed here also predict that the number of micro-cracks should increase as stress increases. However, the models fail to explain the strong dependence of number of cracks on stress that is observed experimentally in Figure 7[6].

The possibility that combined stresses on cleavage planes are a factor in crack nucleation[9] was also investigated. It was found that both root-mean-square and linear sum values of normal and shear stress would tend to bias microcrack formation toward the appearance of higher angle surface traces than is observed experimentally[6].

Consequently, it appears that the very strong dependence of micro-crack formation on stress is not in good agreement with any of the simpli-fied models for microcrack formation that exist at present. This is not to say that the models, which all have the form of eqn. (1), are incor-rect, but rather that they are incomplete. For example, it is known that ferrite microcracks are nucleated at a certain fraction of the cracks in grain boundary carbides[5]. Reduction in the size and number of grain boundary carbides (e.g., by the addition of manganese) leads to an increase in fracture strength and toughness of ferrite[10,11]. This fact would indicate that γ_m is lower when ferrite microcracks are ini-tiated at a cracked carbide than when they are initiated at a virgin

grain boundary.

If, for example, the number of carbide cracks is strongly dependent upon stress, and a certain fraction of carbide cracks, which may, in turn, depend on the stress and length of the carbide cracks, can grow into the ferrite, then the number of ferrite cracks would also be strongly dependent upon stress. The thickness and orientation distribution of the carbides will affect, in some manner yet to be determined, the stress dependence of carbide cracking, while the orientations of the carbide cleavage plane relative to the blocked slip plane on one side and the ferrite cleavage plane on its opposite side will affect the probability that a carbide crack can spread into the ferrite.

For example, McMahon and Cohen[5] have suggested that a carbide crack may propagate into a ferrite grain (γ_m low) as a Griffith crack if the orientation of the carbide crack and a cleavage plane in the ferrite grain are favorable. According to the Griffith relation, the normal stress across the cleavage plane, required for propagation, should then be proportional to $\ell^{-\frac{1}{2}}$ where ℓ is the carbide crack length. If, during an incremental stress increase, the number of carbide cracks formed with length greater or equal to ℓ, $N(\ell)$, is proportional to the inverse fourth power of crack length, then

$$\frac{dN(\ell)}{d\sigma} \propto \frac{1}{\ell^4} \tag{19}$$

The length above which propagation into the ferrite can occur is proportional to the inverse square of the stress level; therefore

$$\frac{dN}{d\sigma} \propto \sigma^8 \tag{20}$$

- 17 -

and $$N \propto \sigma^9 \qquad\qquad (21)$$

in agreement with the experimental results obtained here. The increase in crack density with increasing grain size (Figure 7) may result, in part, from the coarser carbides that existed in the coarse grained material, as well as from the increased length of dislocation pile-ups.

Clearly, more experimental work is needed to determine the stress, size, and orientation dependence of carbide cracking. In view of the small size of carbide cracks, these experiments will be extremely tedious. Furthermore, surface observation of the thickness distribution of carbides does not necessarily give the true thickness distribution, and the orientation of a carbide crack cannot be determined from the surface trace. Statistical analyses similar to those developed here will probably be required to elucidate the role of carbide parameter distributions in microcrack formation.

V. SUMMARY AND CONCLUSIONS

1) A statistical analysis indicates that the true orientation distribution of microcracks is quite different from the observed surface trace distribution.

2) The orientation distribution of microcracks in ferrite is independent of stress, strain and test temperature over the ranges investigated.

3) Measurements of both the microcrack orientation distribution at a given stress level and the total number of microcracks observed at different stress levels indicate that the crack density increases as the ninth power of the normal stress across the cleavage plane. In

ferrite, the crack density increases with increasing grain size at a given stress level.

4) These results do not agree with simple dislocation models of micro-crack formation, which predict a critical stress dependence of micro-crack formation. It is proposed that the discrepancy is related to a size distribution effect in carbide cracks, as it is known that ferrite microcracks initiate at cracked carbides.

REFERENCES

1. A. N. Stroh, *Advances in Physics*, 6, 418 (1957).

2. A. H. Cottrell, *Trans. AIME*, 212, 192 (1958).

3. A. S. Tetelman and A. J. McEvily, Jr., *Fracture of Structural Materials*, Wiley, New York (1967).

4. G. T. Hahn, B. L. Averbach, W. S. Owen and M. Cohen, *Fracture*, p. 91, Wiley, New York (1959).

5. C. J. McMahon, Jr. and M. Cohen, *Acta Met.*, 13, 591 (1965).

6. L. E. Kaechele, *A Statistical Investigation of Cleavage Microcrack Formation in Polycrystalline Iron*, Ph.D. Dissertation, Stanford University (1967).

7. H. Cramer, *Mathematical Methods of Statistics*, Princeton University Press (1946).

8. C. S. Barrett and T. B. Massalski, *Structure of Metals*, McGraw-Hill, New York (1966).

9. R. Priestner and R. F. Krause, *Trans. AIME*, 236, 1246 (1966).

10. N. P. Allen, et. al., *J. Iron Steel Inst.*, 174, 108 (1953).

11. G. T. Hahn, M. Cohen, and B. L. Averbach, *J. Iron Steel Inst.*, 200, 634 (1962).

12. E. T. Whittaker and G. N. Watson, *A Course of Modern Analysis*, Cambridge University Press (1927).

FIGURE CAPTIONS

Figure 1   Angular notation for crack planes and surface traces.

Figure 2   Surface trace of microcrack after removal of 3 mils by grinding and electropolishing. Tested at -180°C, tensile axis in long direction. X830.

Figure 3   Temperature variation of test material properties. Flagged symbols tested at 0.17/min strain rate, unflagged at 0.42/min.

Figure 4   Microcrack count data.

Figure 5   Cumulative distributions of surface trace angles.

Figure 6   Comparison of predicted trace angle distribution from stress power model with experimental trace angle distribution.

Figure 7   Microcrack density vs. maximum uniform true stress. (Flagged symbols for 120 micron grain size, unflagged for 80 micron.)

Figure 8   Microcrack density vs. uniform plastic strain.

Figure 9   Probability distribution of orientation of cleavage plane most nearly normal to the tensile axis for random grain orientation.

Figure 10   Probability distribution for crack plane orientation, $p(\emptyset)$, and for trace angles, $p(\alpha)$, from the critical stress model compared with experimental trace angle histogram (probabilities per degree).

Figure 11   Probability distribution for crack plane orientation, $p(\emptyset)$, and for trace angles, $p(\alpha)$, from the linear stress model compared with experimental trace angle histogram (probabilities per degree).
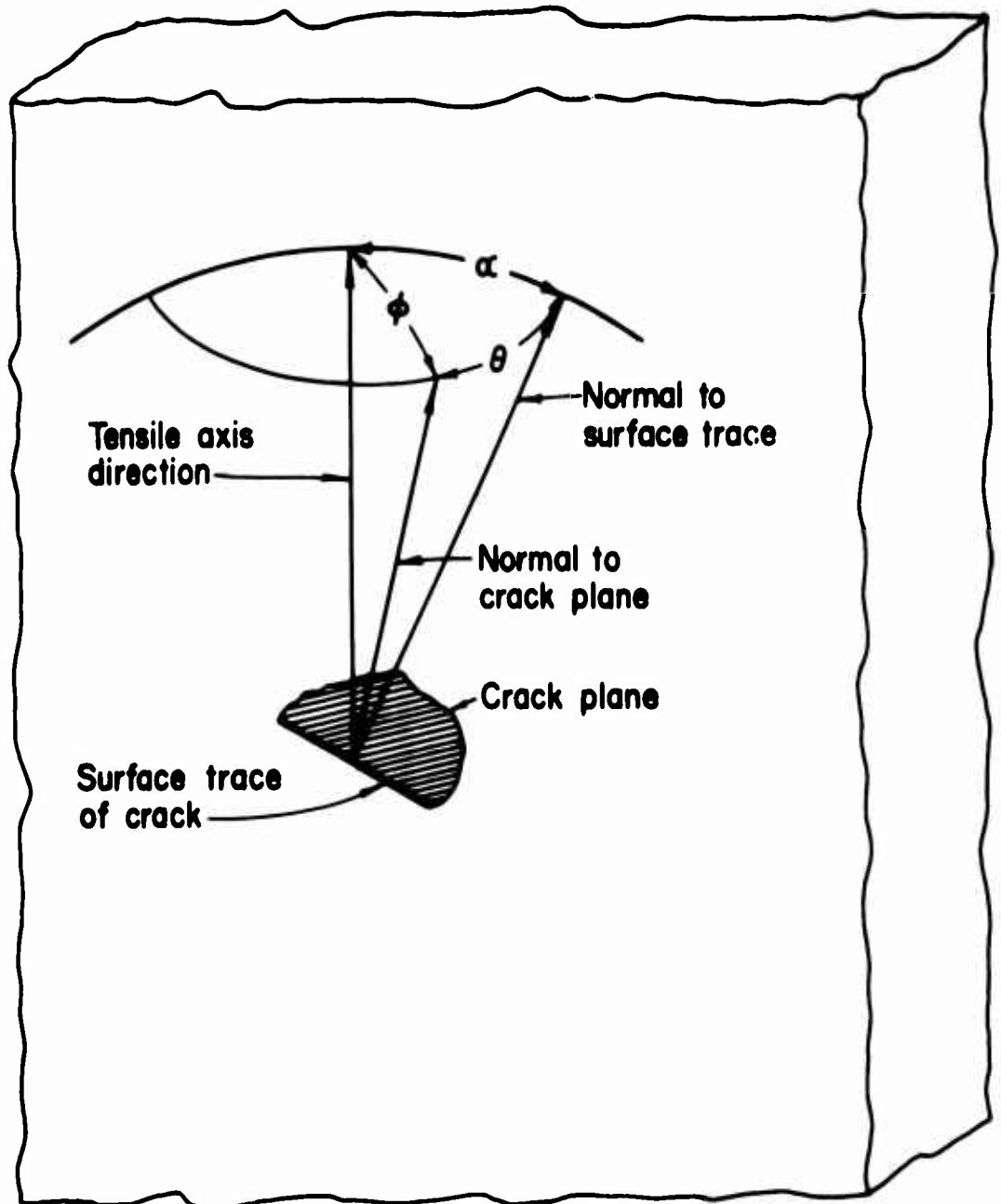
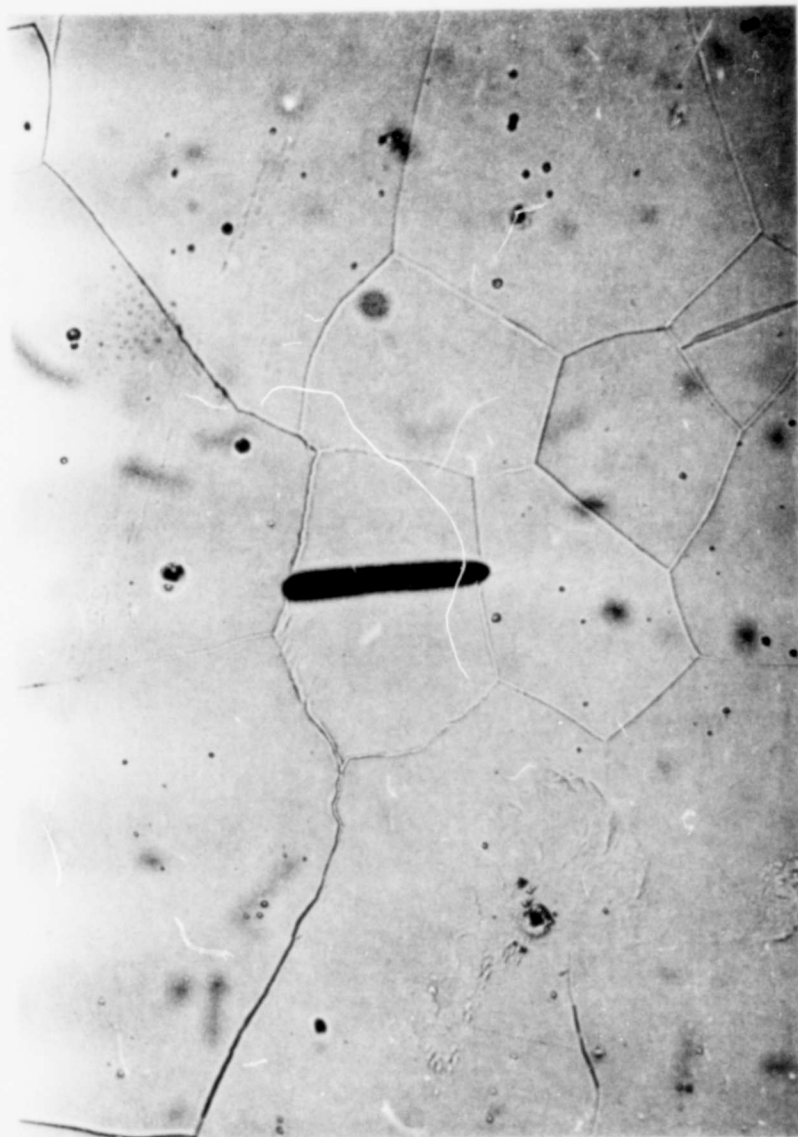Figure 1   Angular notation for crack planes and surface traces.

Figure 2   Surface trace of microcrack after removal of 3 mils by grinding and electropolishing. Tested at -180°C, tensile axis in long direction. X830.
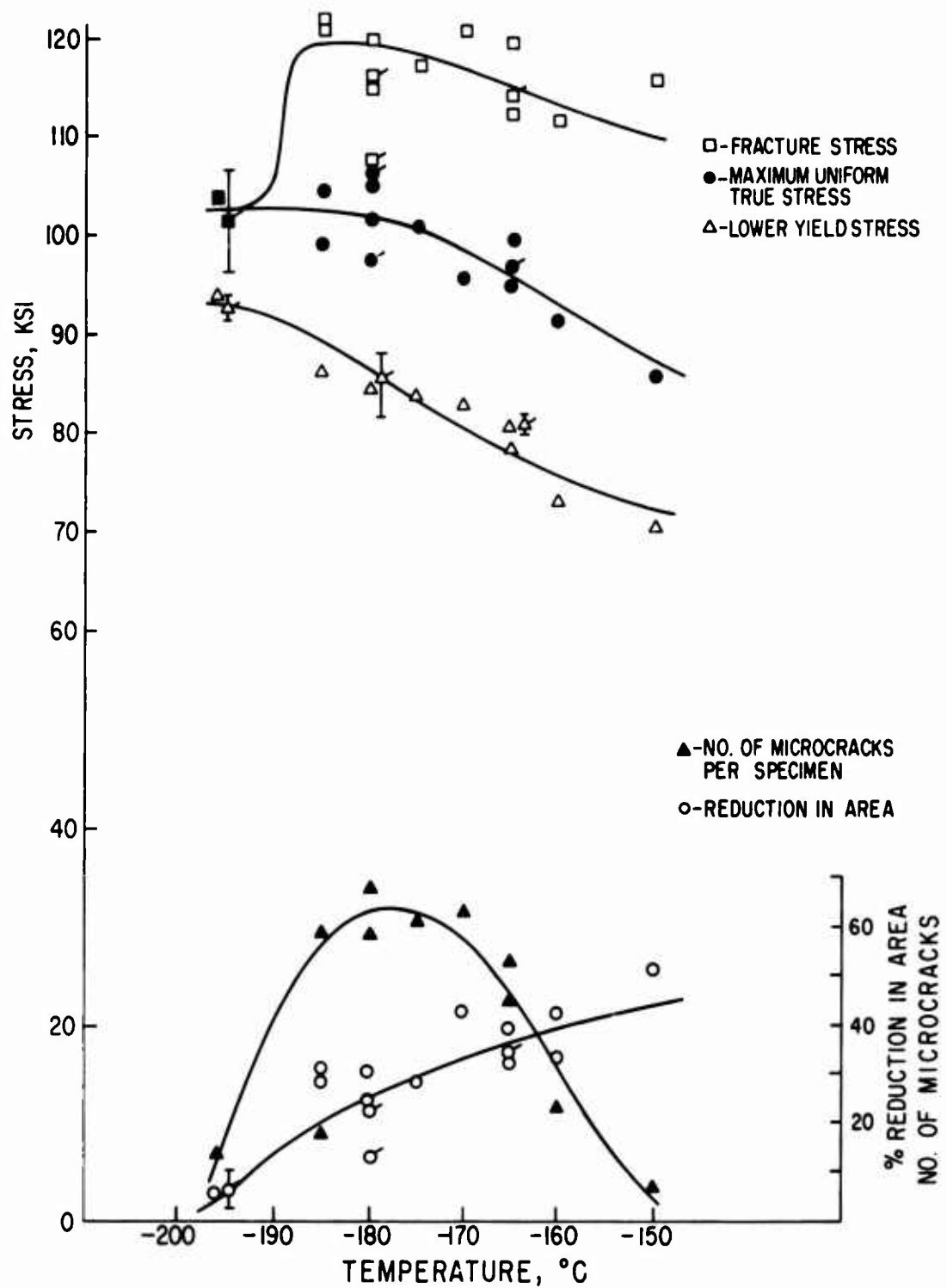
Figure 3   Temperature variation of test material properties. Flagged
symbols tested at 0.17/min strain rate, unflagged at 0.42/min.

Figure 4   Microcrack count data.

Specimen Number	Maximum Uniform True Stress, KSI	Uniform Plastic Strain, %	Number of Microcracks with Trace Angle, in Interval (degrees)											Total Number of Microcracks	Microcracks per Square Inch
			0-5	5-10	10-15	15-20	20-25	25-30	30-35	35-40	40-45	45-50	>50		
			Tests at -165°C												
47	98.2	14.8	90	75	54	37	11	11	1	4	1	1		285	580
48	88.6	7.7	52	41	29	17	7	2	2					150	340
51	93.8	8.5	66	58	44	31	14	1	6	1		1		222	493
53	100.5	14.4	95	79	50	27	19	9	3	2	1		1	285	595
54	97.2	12.5	98	94	49	41	26	14	5	3				331	688
55	96.2	11.1	79	67	61	32	10	9	3	1	1		1	264	590
			Tests at -180°C												
38	107.5	17.1	126	120	104	60	28	22	14		2			476	985

												331	688
55	96.2	11.1	79	67	49	61	41	32	26	14	9	5	3	1	1	264	590

Tests at -180°C

38	107.5	17.1	126	120	104	60	28	22	14	2			476	985
40	89.7	6.5	41	33	20	22	10	2	2				130	525
56	99.4	9.7	86	93	58	35	22	15	6	1		1	317	678
57	108.7	12.4	162	155	97	83	53	25	17	4	2		598	1225
59	105.7	13.2	168	124	106	73	31	21	11	4	1	1	540	1075
60	103.6	12.5	156	130	93	67	36	14	10	3	1	1	510	1045
61	100.8	15.0	87	74	71	32	21	9	9	5	1		305	585

Tests at -196°C

41	105.8	6.4	145	117	79	47	37	16	5	2	1		451	958
42	106.8	5.9	114	94	65	53	22	16	2	2	1	1	369	935
43	101.2	4.8	82	68	52	32	18	13	3	3			271	755
44	96.5	3.0	19	21	9	7	5	6	1				68	433
46	98.4	4.7	65	51	35	27	9	7	1	3	1		199	485
49	103.1	5.3	107	81	61	31	23	14	3	3	1		325	980
52	100.5	5.1	41	42	26	16	5	7	3				140	370*
58	99.0	4.5	38	29	26	17	10	6	4	2			132	585

* Adjustment for area without cracks changes this count to 545.
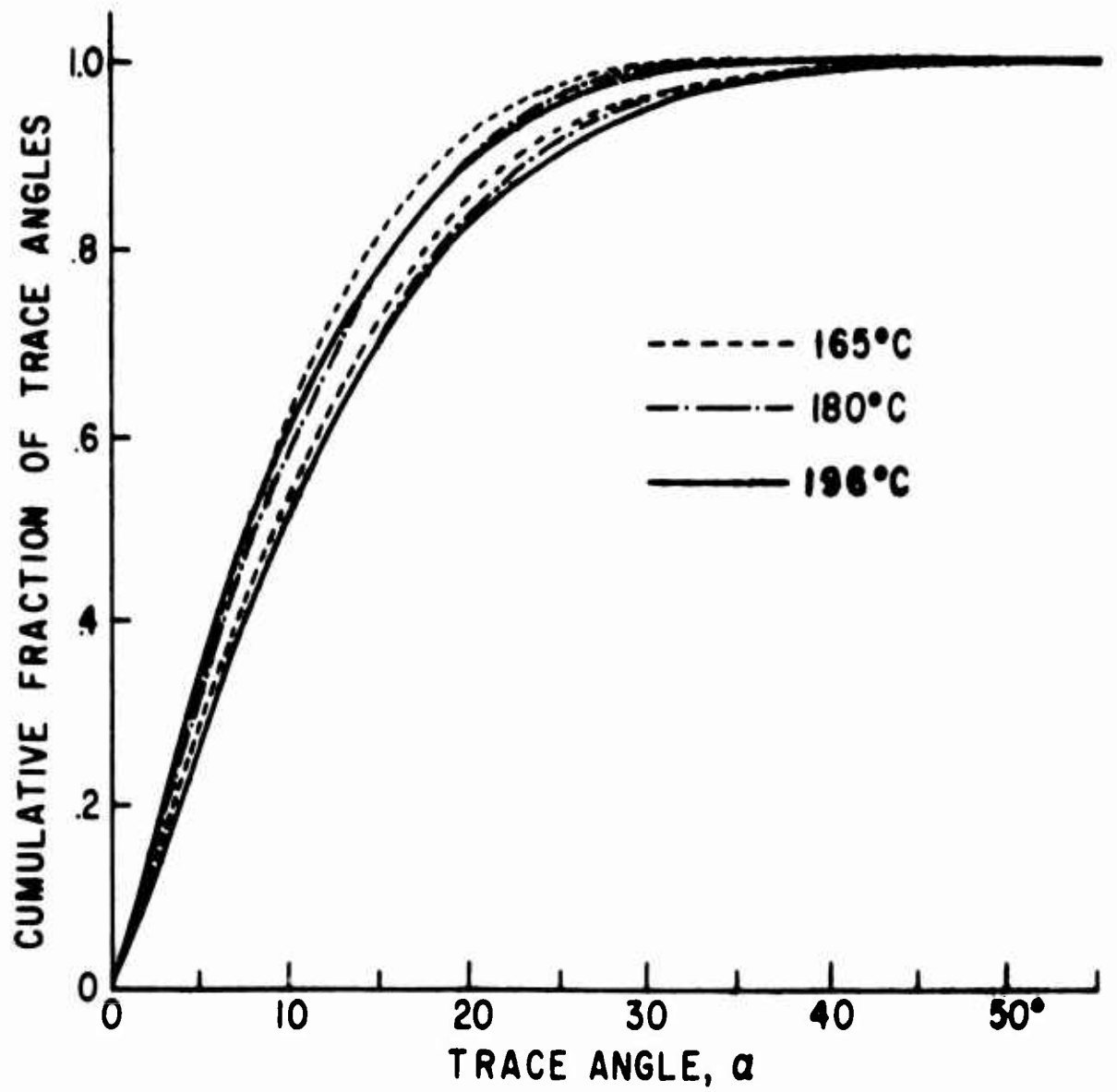
Figure 5   Cumulative distributions of surface trace angles.
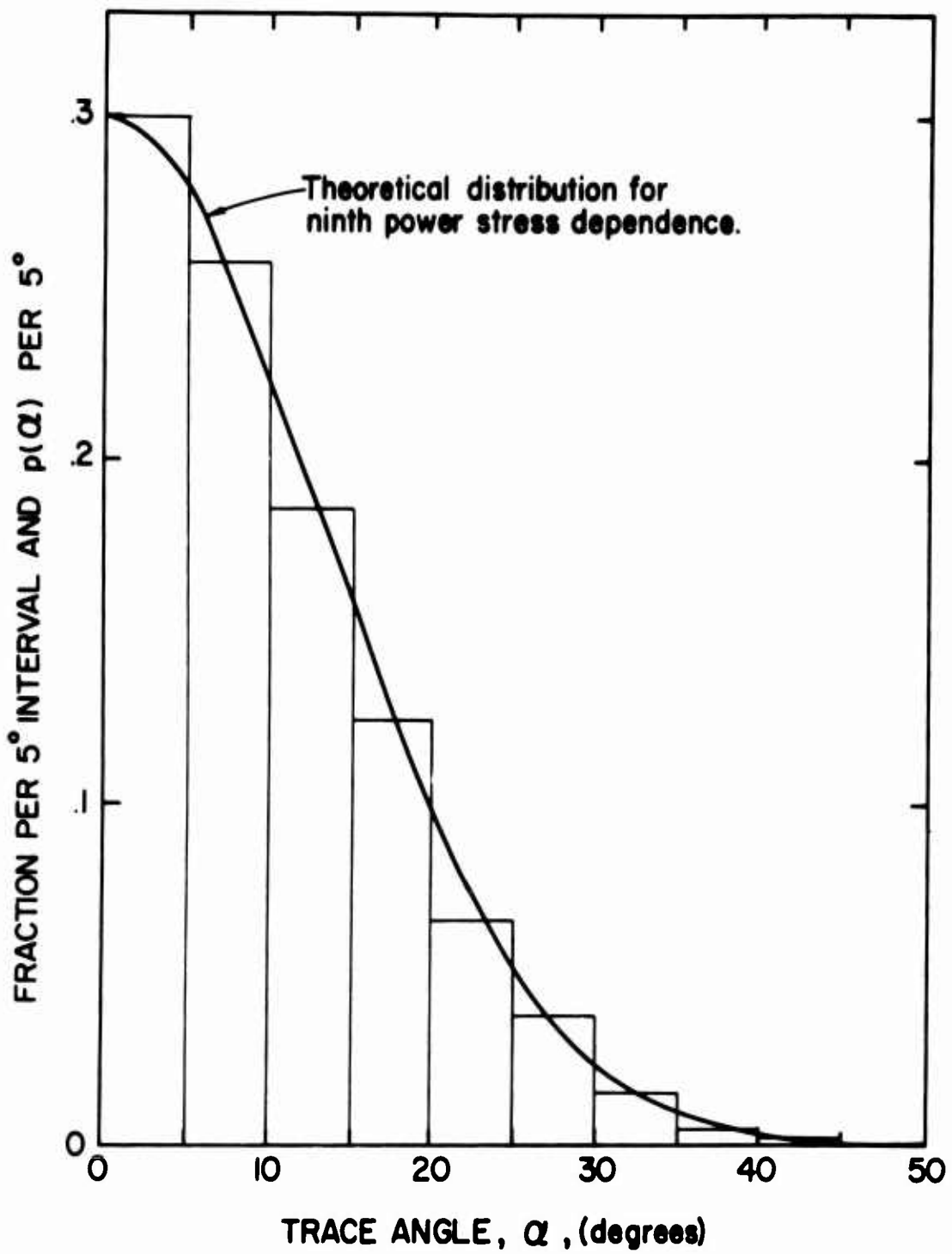
Figure 6   Comparison of predicted trace angle distribution from stress
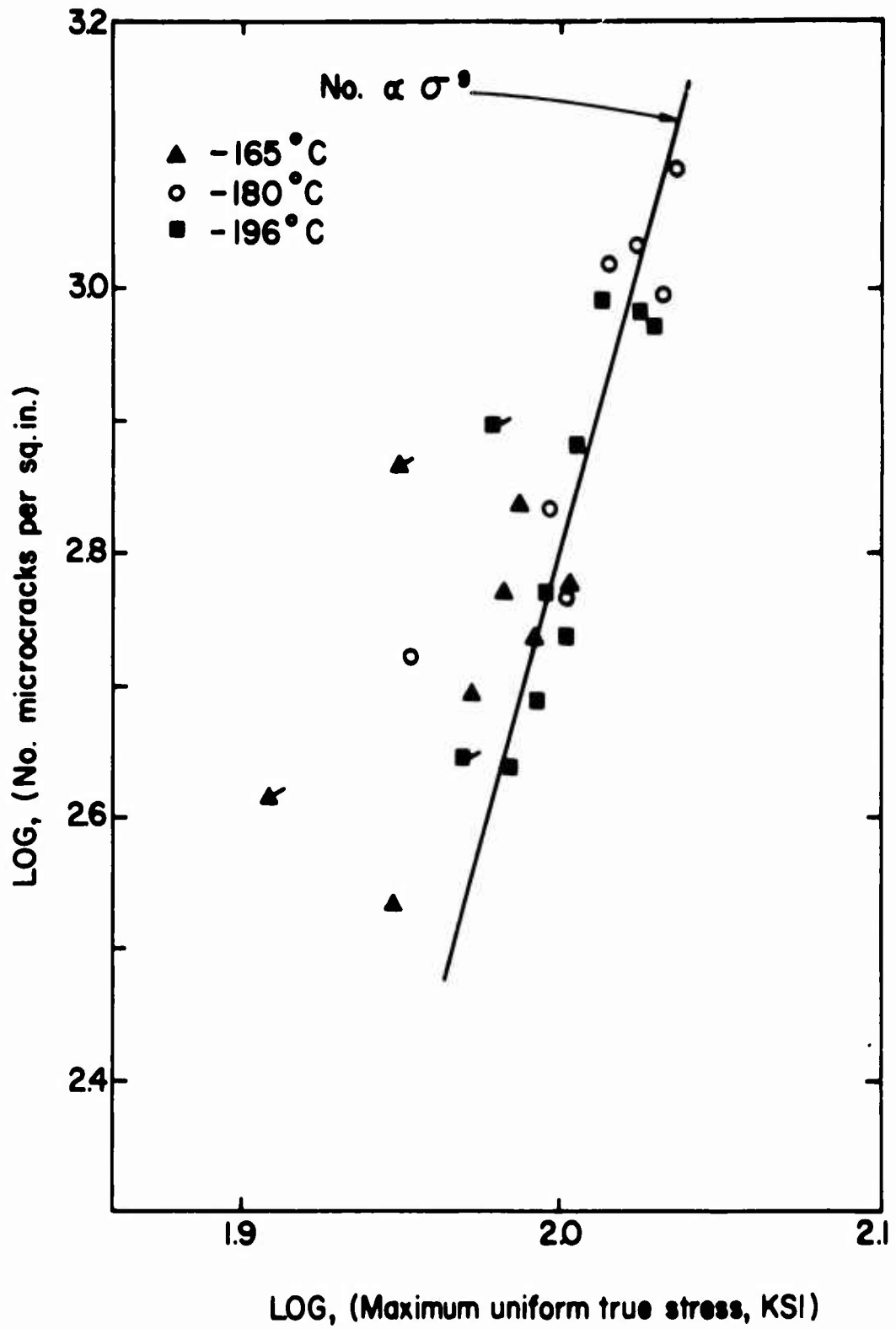power model with experimental trace angle distribution.

Figure 7   Microcrack density vs. maximum uniform true stress.
(Flagged symbols for 120 micron grain size, unflagged
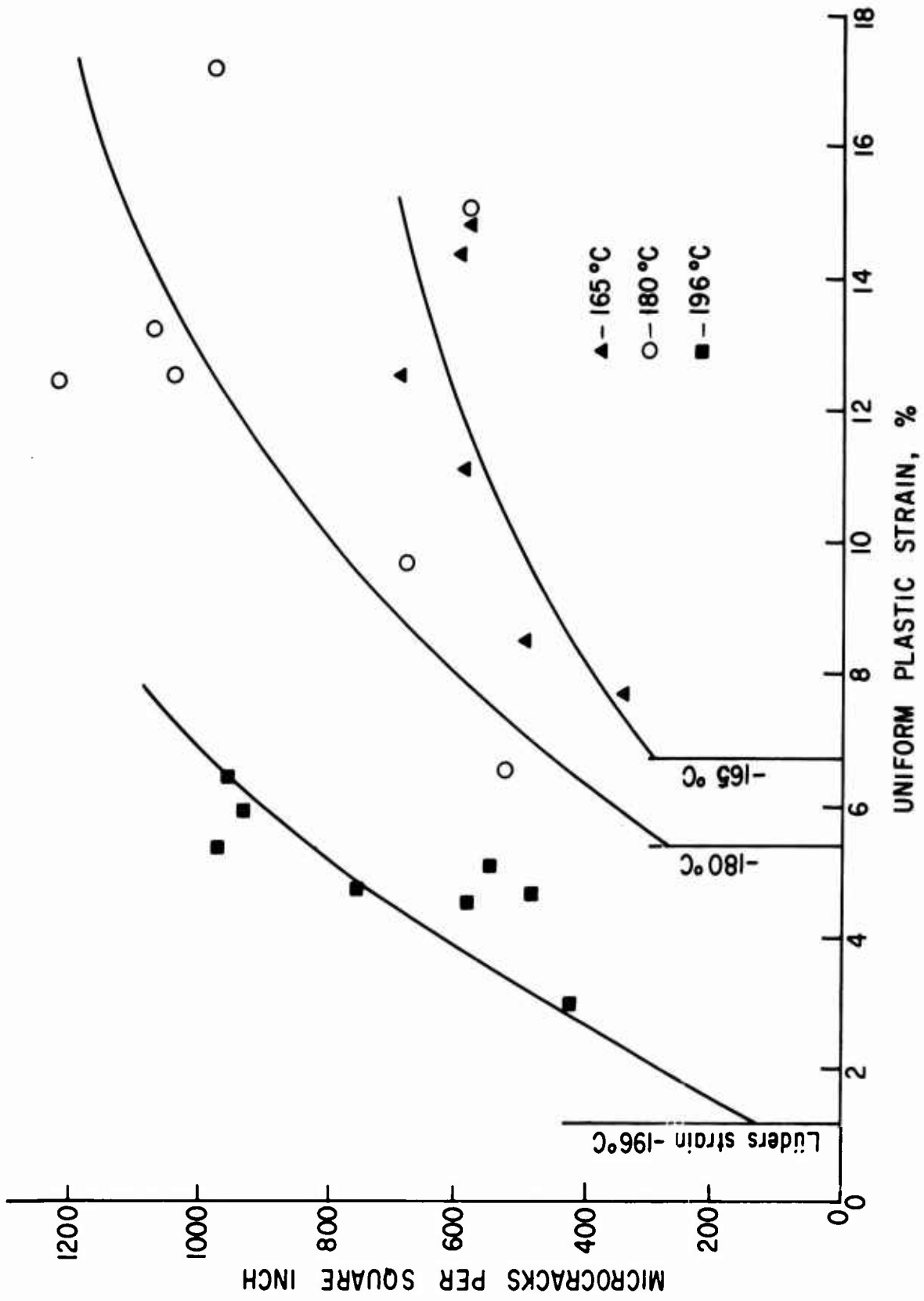for 80 micron).

Figure 8   Microcrack density vs. uniform plastic strain.
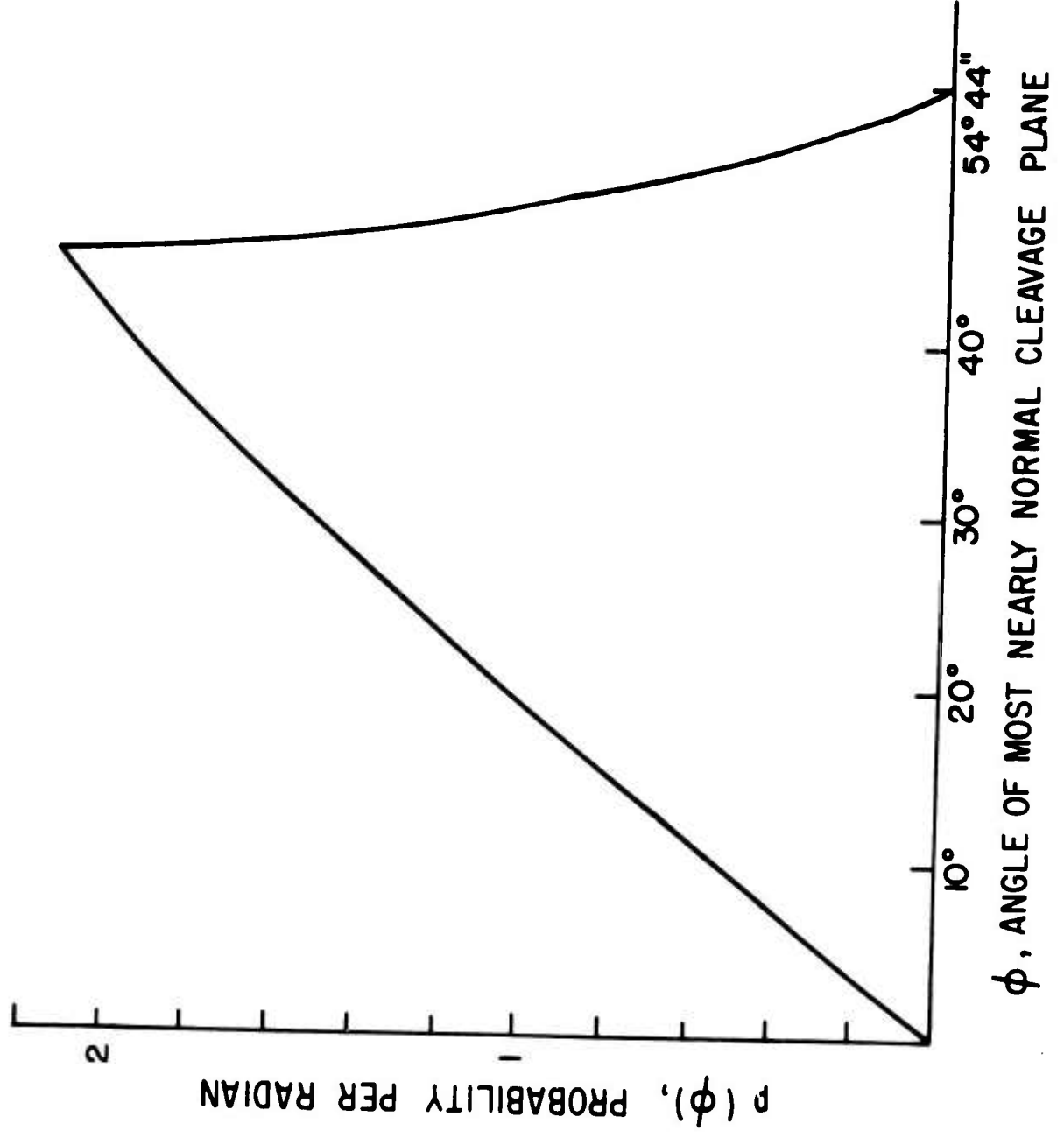
Figure 9   Probability distribution of orientation of cleavage plane most nearly normal to the tensile axis for random grain orientation.
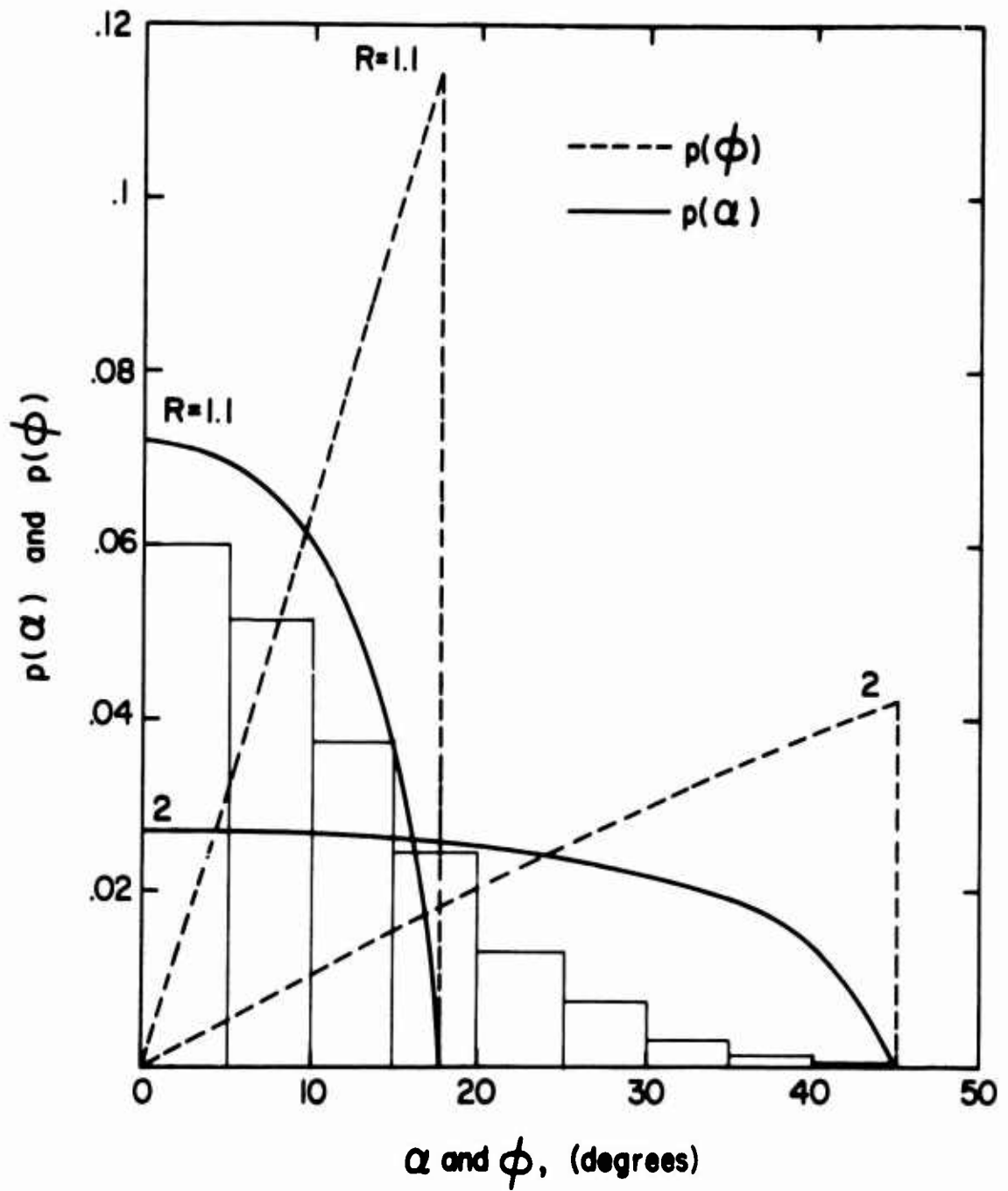
Figure 10   Probability distribution for crack plane orientation,
p(∅), and for trace angles, p(α), from the critical stress
model compared with experimental trace angle histogram
(probabilities per degree).

Figure 11   Probability distribution for crack plane orientation,
p($\emptyset$), and for trace angles, p(α), from the linear stress
model compared with experimental trace angle histogram
(probabilities per degree).

APPENDIX
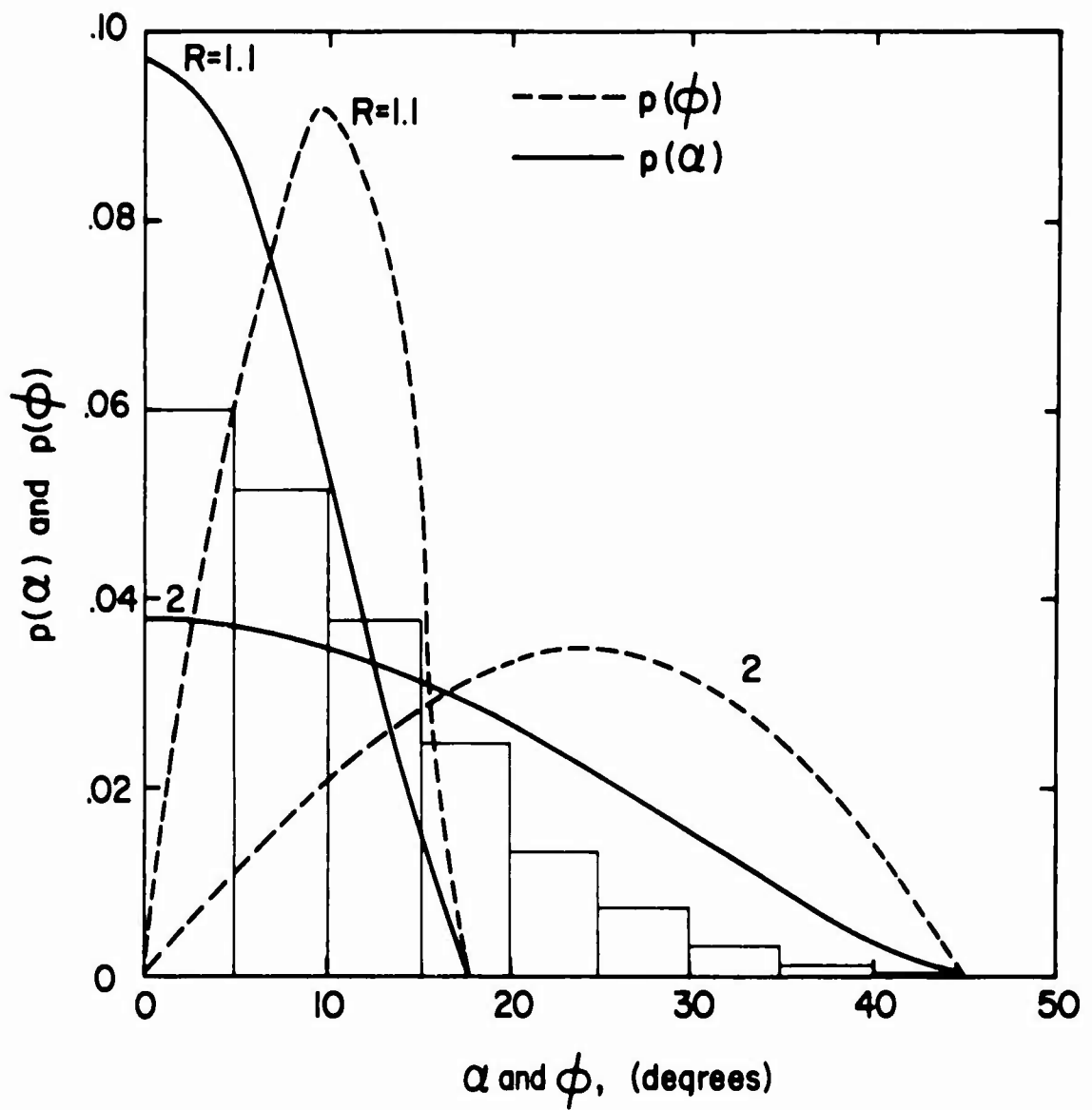
PROBABILITY DISTRIBUTION RELATIONSHIPS BETWEEN MICROCRACK

ORIENTATION AND SURFACE TRACE ORIENTATION

The orientation of microcracks is an important characteristic since their formation depends on factors that vary with orientation. Data on microcrack orientation has been obtained by measuring the angle between the trace made by a crack on the surface of the specimen and some reference axis[4,5]. However, measurement of surface trace angles does not provide information on the true orientation of a microcrack, e.g., the angle between the normal to the crack surface and the loading direction in a tension test (Figure 1).

Denoting this angle by φ, the orientation of microcracks in a specimen can be described by a probability distribution for φ. Such a distribution results from a theoretical analysis of microcrack formation when angular variation of the stress, strain and crystallographic features is included. However, the distribution of angles of surface traces $\propto$ that corresponds to the φ distribution is not immediately evident.

With $\propto$ the angle between the tensile axis and the normal to the surface trace of a crack, $\emptyset$ the angle between the tensile axis and the normal to the crack surface, and θ the angle by which the crack surface normal is rotated around the tensile axis, out of the plane of the surface, from geometrical relationships,

$$\tan \propto = \cos \theta \tan \emptyset . \tag{A1}$$

If the distribution of crack plane normals is uniform with respect to

rotation, θ, only one quadrant of θ need be considered, and the probability of a crack plane normal lying between $\emptyset$ and $\emptyset + d\emptyset$ and also between θ and $\theta + d\theta$ is

$$p(\emptyset) \; d\emptyset \; \frac{d\theta}{\pi/2} \; . \tag{A2}$$

From eqn. (A1) it can be found that

$$d\theta = - \frac{d\alpha}{\cos^2 \alpha \; \sin \theta \; \tan \emptyset} = \frac{- \cos \emptyset \; d\alpha}{\cos \alpha \; \sqrt{\cos^2 \alpha - \cos^2 \emptyset}} \; . \tag{A3}$$

Substituting this in eqn. (A2), the contribution to the probability distribution of trace angles from that equation is

$$\frac{p(\varphi) \; \cos \emptyset \; d\emptyset \; d\alpha}{\cos \alpha \; \sqrt{\cos^2 \alpha - \cos^2 \emptyset}} \tag{A4}$$

and thus the probability that a crack trace will be found between α and $\alpha + d\alpha$ is

$$p(\alpha) = \left| \frac{2}{\pi} \int_{\alpha}^{\pi/2} \frac{p(\emptyset) \; \cos \emptyset \; d\emptyset}{\cos \alpha \; \sqrt{\cos^2 \alpha - \cos^2 \emptyset}} \right| \tag{A5}$$

for a specified probability distribution of the orientation of the normals to interior cracks, $p(\varphi)$.

The converse form of this relationship, that determines the distribution of crack plane normals that must exist inside a specimen in order to account for the distribution of observed surface trace angles, is presented below.

The desired relationship is found by making a substitution of variables in the equation found previously for determining trace angle distribution, to give a standard form of integral equation for which a

A-2

solution is known[6]. This relationship is unique if the distribution of crack normals is uniform with respect to rotation about the reference axis and the effect of cracks not centered on the surface is neglected. (The number of cracks observed must be large enough to make the angle distributions statistically significant.)

By making the substitution

$$x = \cos^2 \alpha \qquad (A6)$$

and

$$t = \cos^2 \varphi \qquad (A7)$$

in eqn. A5, and with $p(\alpha(x))$ representing the probability function for α with α expressed in terms of x, and similarly for $p(\varphi(t))$, and defining

$$p^*(\varphi(t)) = \frac{p(\varphi(t))}{\sqrt{1-t}} \qquad (A8)$$

eqn. A5 can be transformed to

$$\pi \sqrt{x} \, p(\alpha(x)) = \int_0^x \frac{p^* \, (\varphi(t)) \, dt}{\sqrt{x-t}} \quad . \qquad (A9)$$

Eqn. A9 is in the form of Abel's equation. Subject to the requirement that the derivative of $p^*(\varphi(t))$ be continuous over the range of integration and that $p^*(\varphi(t))$ be equal to zero at the lower limit of the integral, the function $p^*(\varphi(t))$ must be[12]

$$p^*(\varphi(t)) = \frac{d}{dt} \int_0^t \frac{\sqrt{x} \, p(\alpha(x)) \, dx}{\sqrt{t-x}} \quad . \qquad (A10)$$

Therefore, from eqn. A8

$$p(\varphi(t)) = \sqrt{1-t} \, \frac{d}{dt} \int_0^t \frac{\sqrt{x} \, p(\alpha(x)) \, dx}{\sqrt{t-x}} \qquad (A11)$$

or

$$p(\varphi(t)) = \sqrt{1-t} \; \frac{d}{dt} \int_0^t \frac{2x \; \sqrt{1-x} \; p(x) \; dx}{\sqrt{t-x}} \quad . \tag{A12}$$

Thus, from an observed distribution of surface trace angles, $p(\alpha)$, the distribution of internal crack orientation, $p(\varphi)$, that must have produced it can be found. Eqn. A11 can be manipulated to eliminate the necessity for differentiation, giving an expression in the integral form[6]. This is

$$p(\varphi(t)) = \frac{\sqrt{1-t}}{t} \int_a^t \left[\left(\frac{3x \; \sqrt{1-x}}{\sqrt{t-x}} - \frac{x^2}{\sqrt{1-x} \; \sqrt{t-x}} \right) p(x) \right.$$
$$\left. + \frac{2x \; \sqrt{1-x} \; p'(x)}{\sqrt{t-x}} \right] dx \tag{A13}$$

where a is defined as

$$a = \cos^2 (\text{maximum value of } \alpha) \; . \tag{A14}$$

If the distribution of surface trace angles is expressed in trigonometric form, the terms from the function and its derivative are frequently found to combine and simplify the integration. Further, the form of eqn. A13 is more suitable for machine computation.

DOCUMENT CONTROL DATA - R & D

(Security classification of title, body of abstract and indexing annotation must be entered when the overall report is classified)

1. ORIGINATING ACTIVITY (Corporate author)	2a. REPORT SECURITY CLASSIFICATION
Stanford University	Uncl
	2b. GROUP N/A

3. REPORT TITLE

A STATISTICAL INVESTIGATION OF MICROCRACK FORMATION

4. DESCRIPTIVE NOTES *(Type of report and inclusive dates)*

Technical Reports

5. AUTHOR(S) *(First name, middle initial, last name)*

Kaechele, L. E.
Tetelman, A. S.

6. REPORT DATE	7a. TOTAL NO. OF PAGES	7b. NO. OF REFS
April 1968	36p	12

8a. CONTRACT OR GRANT NO.	9a. ORIGINATOR'S REPORT NUMBER(S)
DA-31-124-ARO-D-251	
b. PROJECT NO.	SU-DMS Report No. 68-T73
20014501B32D	
c.	9b. OTHER REPORT NO(S) *(Any other numbers that may be assigned this report)*
d.	4800.12-MC

10. DISTRIBUTION STATEMENT

11. SUPPLEMENTARY NOTES	12. SPONSORING MILITARY ACTIVITY
None	U.S. Army Research Office-Durham Box CM, Duke Station Durham, North Carolina 27705

13. ABSTRACT

Low temperature tension tests were made with low carbon poly-crystalline iron, in which stable cleavage microcracks form. Probability distributions of the orientation of these cracks were used to investigate the effects of stress and strain on their formation. Since only the surface traces of cracks could be observed experimentally, relationships were developed to give the distribution of the true orientation of these cracks as measured by the direction of the normal to the crack plane. Simple models for the effect of stress on crack formation were investigated, including the Cottrell-Petch formulation for microcrack formation. Predictions of the probability distribution of crack orientation angles, and from these the distribution of the surface trace angles that should be observed experimentally, were determined for these models.

14. KEY WORDS

polycrystalline iron
microcracks
stress
crack formation
crack orientation angles
surface trace angles